CHEMISTRY OF MATERIALS

ARTICLE

pubs.acs.org/cm

Controllable Morphology of Engelhard Titanium Silicates ETS-4: Synthetic, Photocatalytic, and Calorimetric Studies

Yin-Qing Zhang,[†,‡] Wei Zhou,[‡] Shuangxi Liu,[*,†] and Alexandra Navrotsky[*,‡]

[†]Institute of New Catalytic Materials Science, College of Chemistry, Nankai University, Tianjin 300071, P. R. China

[‡]Peter A. Rock Thermochemistry Laboratory and NEAT ORU, University of California at Davis, Davis, California 95616, United States

ABSTRACT: Titanosilicate ETS-4 materials with three different morphologies were synthesized hydrothermally by controlling the pH of the synthesis gel mixtures. Their morphology changed from thin rectangular plate monolithic crystals to double-fan-like polycrystalline aggregates as the pH decreased. The crystallization time depended on the initial pH. The effect of morphology on photocatalytic activity was investigated using the photodegradation reaction of Rhodamine B under visible light irradiation. The double-fan-like material exhibited significantly greater photodegradation activity than the other two ETS-4 samples and Degussa P25 titania. Powder X-ray diffraction, electron microprobe analysis, scanning electron microscopy, Raman spectroscopy, and diffuse reflectance ultraviolet−visible spectroscopy were performed to find possible reasons for the photocatalytic activity difference of the three samples. The enthalpies of formation from oxides for all the ETS-4 materials were investigated by high temperature oxide melt calorimetry. The results showed that the three samples with different morphologies have differences in their enthalpies of formation, which, although small, are bigger than likely to arise from surface area effects alone, and the product with most Ti−OH groups has the smallest thermodynamic stability. The calorimetric and spectroscopic data together provide evidence that the high photocatalytic activity of the double-fan-like aggregates is linked to their high Ti−OH content.

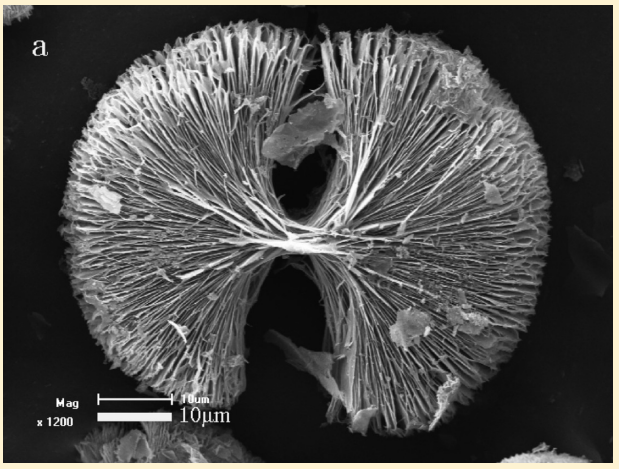

KEYWORDS: ETS-4, morphology, photocatalysis, calorimetry, enthalpy of formation

1. INTRODUCTION

Photocatalysis has received extensive attention in recent years for its applications in organic synthesis[1,2] and the abatement of pollutants in water and air.[3−5] Titanium dioxide (TiO_2) is one of the most widely studied photocatalysts for applications in several fields and particularly for its great performance in water splitting and oxidative photodegradation of many organic pollutants.[6−8] However, because of the large band gap (3.0 eV for the rutile phase and 3.2 eV for the anatase phase), TiO_2 can only adsorb light with wavelength shorter than 388 nm, which is only 3−4% of the solar energy that reaches the Earth.[9] Therefore, many researchers have sought more efficient photocatalysts by the modification of titanium dioxide.[10−13]

Organic dye pollutants that absorb visible light are produced by the textile and photographic industries, and their influence on the environment is of increasing concern. There are now many reports on photodegradation of such dyes using TiO_2-based photocatalysts.[14−18] However, the mechanism of photodegradation can be different depending on whether UV or visible light is used for the photoillumination. If visible light is used, the dye itself can be photoexcited (sensitized) and electron transfer may then occur from the excited dye molecule into the conduction band of the semiconductor.[19]

Microporous titanosilicates comprise a new family of molecular sieve materials that possess zeolite-like properties such as catalysis, separation, absorption, and ion exchange. They usually consist of $[TiO_6]$ octahedra (or possibly $[TiO_5]$ square-pyramids) and $[SiO_4]$ tetrahedra. The different coordinations of Ti^{4+} and Si^{4+} produce unique framework topologies. The different pore and channel structures in titanosilicates provide this group of materials some unique properties and thus potentially novel applications.[20] Engelhard titanium silicates (ETS) including ETS-4 and ETS-10 are a class of zeolite-type titanosilicate materials[21,22] characterized by the presence of one-dimensional linear chains of TiO_6 octahedra (−O−Ti−O−Ti−) that exhibit quantum confinement effects and behave as semiconductor nanowires in the framework.[23−25] For ETS-10, electronic communication can occur between the −O−Ti−O−Ti− semiconductor

Received: September 10, 2010
Revised: January 4, 2011
Published: January 21, 2011

chains and guest species in the pores. The photocatalytic activity of these materials in the oxidation of organic compounds has been studied.[26−29] As reported by Zecchina's group,[28] terminal Ti−OH groups of the −O−Ti−O−Ti− chains play an important role in improving the photocatalytic performance of ETS-10. Compared to ETS-10, less attention has been paid so far to the photocatalytic properties of ETS-4. Guan's group loaded Pt and Au onto ETS-4 zeolites and showed stable photocatalytic activity for H_2 evolution from water.[30] In the ETS-4 framework, the −O−Ti−O−Ti− chains run zigzag along the *b* axis, with neighboring octahedra in a chain being laterally linked by [SiO_4] tetrahedra. Pairs of [SiO_4] tetrahedra are further joined via a bridging unit containing one titanium pyramid [TiO_5].[31,32] Thus, ETS-4 can be considered as a set of one-Ti-wide wires of titanium dioxide embedded into an insulating siliceous matrix. Since the amount of terminal titanols depends on the size and morphology of the crystals, it can be raised by means of morphology controlling treatments.

We present here results concerning the morphology-controlled synthesis of ETS-4 by changing the initial pH. All the raw materials are simple environmentally benign inorganic chemicals. No organic template or structure directing agent was used in the synthesis. The aims of this synthesis of well-defined ETS-4 are to minimize the use and generation of hazardous substances and to use ETS-4 to decontaminate chemical pollutants in wastewaters. X-ray diffraction (XRD) and scanning electron microscopy (SEM) have been applied to detect possible changes in the crystallinity and the morphology of the products. The relationship between the crystallization kinetics of ETS-4 and the pH of the synthesis mixture has also been investigated. Rhodamine B is a common model dye in the triphenylmethane family, which is unable to penetrate inside the zeolitic pores. The photocatalytic degradation reaction of Rhodamine B under visible light irradiation has been investigated to test the photocatalytic activity of the prepared ETS-4 materials. The results have been compared to those obtained by using the commercial TiO_2 Degussa P25 as a photocatalyst. Raman spectroscopy and diffuse reflectance UV−visible (DRUV−vis) spectroscopy in the presence of H_2O_2 were used to study the relation between the morphology and the amount of Ti−OH groups of the ETS-4 materials. In addition, high temperature oxide melt calorimetry was employed to evaluate the energetics of these ETS-4 photocatalysts. The enthalpies of formation from oxides, the thermodynamic stability, and the implications for photocatalytic activity are discussed. The goals of the simultaneous use of spectroscopic characterization and solution calorimetry are to provide an indication of the overall stability of the ETS-4 materials during photocatalysis and to identify the sources of any differences in photocatalytic activity among the different samples.

2. EXPERIMENTAL METHODS

2.1. Materials. Titanium(IV) sulfate solution (18.0 wt %) was purchased from Tianjin Third Chemical Co., Ltd., and silica sol (30.0% SiO_2) was obtained from NanKai Chemical Factory. Sodium hydroxide was of analytical grade, and sulfuric acid was diluted to make a 1.0 M stock solution. All chemicals were used as received unless otherwise specified.

2.2. Synthesis Procedure. All the ETS-4 materials were synthesized via a hydrothermal method. The molar compositions of gels were xNa_2O: $3.6SiO_2$: $1TiO_2$: yH_2SO_4: $240H_2O$, where $x = 9.0−8.2$ and $y = 0−0.24$. Synthesis mixtures were formed by combining two precursor solutions, one containing titanium(IV) sulfate, sulfuric acid, and deionized water, the other containing silica, sodium hydroxide, and deionized water. In a typical preparation ($x = 8.2$, $y = 0.24$, while for others $y = 0$), 16.0 g of sodium hydroxide was dissolved in 30.0 mL of deionized water. After cooling down to room temperature, 17.6 mL of silica sol was added to this solution to form the silicon-contained precursor solution. The titanium-containing precursor solution was prepared by mixed 36.8 mL of titanium(IV) sulfate solution with 6.00 mL of sulfuric acid and 30.0 mL of deionized water. Then the two precursor solutions were mixed under vigorous mechanical stirring for 15 min to form an initial synthesis gel. The pH of the mixture was measured using a Mettler Toledo Delta 320 pH meter. The gel was then transferred into nine Teflon-lined stainless steel autoclaves, which were then sealed and kept at 448 K for various durations up to 15 days. After the reaction, the autoclave was cooled under cold tap water. The resulting powders are filtered, washed with deionized water, and dried at 343 K for 24 h in air. Gels with three pH values (13.00, 12.70, and 12.30) were used in this study, and the corresponding 100% crystallized products were designated as ETS-4-1, ETS-4-2, and ETS-4-3.

2.3. Characterization. Powder X-ray diffraction (XRD) data were collected on a Rigaku D/MAX-2500 diffractometer with monochromatic Cu Kα radiation operated under 40 kV and 100 mA. All the samples were scanned from 5°−45° 2θ with a scan rate of $1°\cdot min^{-1}$. The ETS-4 samples were ground before the XRD measurements to minimize the effect of preferred orientation on the XRD pattern. The crystallization kinetics was studied by performing XRD on samples with different crystallization times. The crystallinity of each sample was calculated by normalizing the integrated intensities of diffraction peaks at $2\theta = 16.8°$, 24.6°, 30.0°, and 30.8° of the sample to those of the 100% crystallized sample.

The compositions of all the samples were determined by electron microprobe analysis using a Czmeca SX-100 with a voltage of 20 kV and a beam current of 10 nA. Compositions were calculated as the average value of 10 analyzed points. The error given is two standard deviations of the mean.

Water contents of all the samples were determined by thermogravimetric analysis (TGA) using a Netzsch Thermal Analyzer STA 409 system with a heating rate of 10 °C/min in static air.

Scanning electron microscopy (SEM) was performed on a Shimadzu SS-550 Superscan instrument at 15 kV. All samples were coated with a conductive layer of sputtered gold prior to the analysis.

Raman spectra were acquired on a Renishaw InVia Raman microscope with a 20 mW Argon ion laser operating at a wavelength of 514.5 nm. Analysis was done at room temperature using a focused beam on the table facet of a randomly oriented sample.

The diffuse reflectance UV−visible (DRUV−vis) spectra were recorded on a Shimadzu UV-2550 UV−visible spectrophotometer equipped with an integrating sphere accessory. Hydrogen peroxide (30% v/v) aqueous solution was dosed to the ETS-4 samples under incipient wetness conditions. After drying at room temperature, we recorded the DRUV−vis data in the range between 300 and 500 nm using a 2-nm slit.

2.4. Photocatalytic Activity. The photocatalytic activities of the ETS-4 samples and the commercial TiO_2 photocatalyst, Degussa P25, were studied by the photodegradation of Rhodamine B under visible light irradiation. The photocatalytic reactions were conducted in a photochemical reactor, which is configured with a light source system, a magnetic stirrer, and 12 silica glass test tubes. Cooled by a water jacketed condenser, a 500 W xenon lamp with six UV cutoff filters was the visible light source.

For a typical photocatalytic reaction, 0.03 g of photocatalyst was added to 20 mL of Rhodamine B solution (20 mg/L) in a quartz test tube. The mixture was stirred for 40 min in dark to ensure the adsorption−desorption equilibrium of Rhodamine B. After that, the mixture was

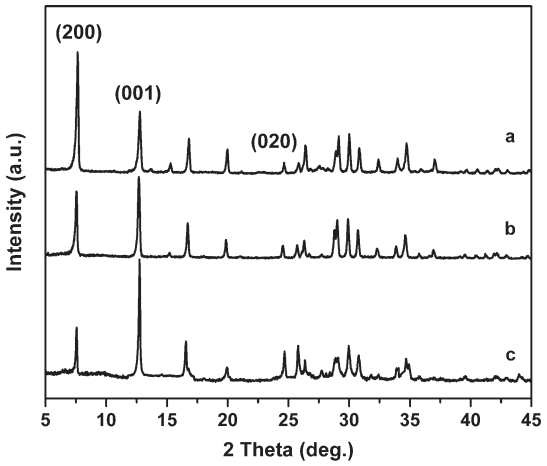

Figure 1. XRD patterns of the three ETS-4 products (a) ETS-4-1, (b) ETS-4-2, and (c) ETS-4-3.

illuminated with visible light under magnetic stirring. After certain given irradiation time, the test tube was taken out, and the solid was separated from the solution by centrifugation at 7000 rpm for 15 min. The concentration of Rhodamine B in the remaining solution was measured by a UV−visible spectrophotometer (Shimadzu UV-2550) at λ_{max} = 554 nm.

2.5. High Temperature Oxide Melt Calorimetry. High temperature solution calorimetric measurements were performed using a custom-built Tian−Calvet twin calorimeter operating at 973 K with molten lead borate ($2PbO \cdot B_2O_3$) as the solvent. The equipment and experimental procedure have been described in detail by Navrotsky.[33,34] The drop solution enthalpy of a sample pellet (about 5 mg) was measured by dropping it from room temperature into the solvent in the calorimeter. To remove the water vapor evolved by dehydration, O_2 gas with a flow rate of 40 mL/min was flushed through the sample chamber of the calorimeter.[35] The measured enthalpy of the drop solution includes the heat content of the sample from room temperature to 973 K, the heat effect of dissolving the sample in the solvent, and that of removing the H_2O. All the water in the sample was evolved into the gas phase, as shown previously.[35−37] The calorimeter was calibrated by using 5 mg α-alumina pellets, whose heat content is known.[38] At least eight pellets of each sample were dropped into the calorimeter. The reported uncertainties are two standard deviations of the mean.

3. RESULTS AND DISCUSSION

3.1. Phase Identification and Chemical Analysis. The powder XRD patterns of the three completely crystallized ETS-4 samples are shown in Figure 1. All the products have patterns characteristic of ETS-4 as referenced in the patent literature.[21] However, there are some small differences in the relative intensities of the peaks in the three XRD patterns. Most noticeable are the changes of the relative intensity of the three peaks at 2θ = 7.6°, 12.7°, and 24.6°, which are the (200), (001), and (020) reflections of ETS-4, respectively. These intensity differences indicate that, compared to ETS-4-1, the [001] and [010] directions are preferred crystallographic orientations in ETS-4-3. The −O−Ti−O−Ti− chains in ETS-4 crystals run along the [010] direction and are connected by silicate tetrahedra in the [001] direction and by either twelve-membered rings or bridging titanosilicate units in the [100] direction.[39,40] Thus, in the ETS-4-3 sample there appear to be more twelve-membered rings terminating on the {001} crystal faces, which can be conducive to trapping more reactant molecules. There are also more −O−Ti−O−Ti− chains running in the [010] direction, which may offer more exposed surface Ti−OH groups. Both of these factors can improve the performance of ETS-4-3 in photocatalytic reactions.

Table 1. Chemical Compositions of the Three ETS-4 Samples

samples	chemical formula	molecular weight (g/mol)
ETS-4-1	$Na_{0.415}Ti_{0.252}Si_{0.645}O_2 \cdot 0.873H_2O$	87.42
ETS-4-2	$Na_{0.402}Ti_{0.252}Si_{0.648}O_2 \cdot 0.828H_2O$	86.41
ETS-4-3	$Na_{0.370}Ti_{0.253}Si_{0.654}O_2 \cdot 0.804H_2O$	85.48

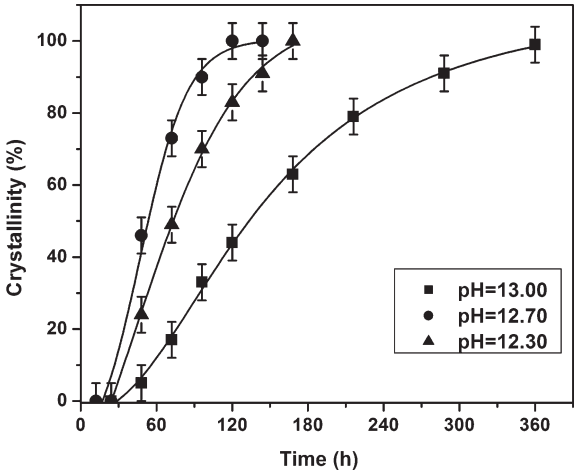

Figure 2. Crystallization curves for ETS-4 grown from synthesis mixtures with different synthesis pH values.

The chemical formulas and the molecular weights on TO_2 (T = Si and Ti) basis are shown in Table 1 obtained from electron microprobe analysis and weight loss experiments. Our results are close to the ideal stoichiometry.[22] The sodium content decreases slightly from ETS-4-1 to ETS-4-3, which may be caused by the difference of the pH in the initial synthesis mixture. The water contents also decrease from ETS-4-1 to ETS-4-3, which is consistent with the trend of the sodium content.

3.2. Crystallization Kinetics. The crystallization curves of the three ETS-4 products are shown in Figure 2. All exhibit the typical sigmoid shape involving two distinct stages, the induction stage to form nuclei, and the crystal growth stage, which has been observed in titanosilicate ETS-4 crystallization.[41−43] The induction time is about 24 h for all syntheses, but the crystallization rates, measured from the slope of the crystallization curves, are different for the three synthesis conditions. At initial pH = 13.00, the crystallization rate is the slowest, and it took 15 days to synthesize the product with 100% crystallinity, which is more than twice the time for the other two products. The fastest crystallization occurred at a pH of 12.70, and the overall crystallization time was only 5 days. For pH 12.30, about 50% of amorphous material converted to ETS-4 crystallites after the first 3 days. Then, the crystallization rate declined gradually, so that the crystalline ETS-4-3 product was obtained after 7 days.

3.3. Morphology Characterization and the pH Effect. The SEM photographs are shown in Figures 3, 4 and 5. The ETS-4 morphology changed from prismatic single crystals to double-fan-like polycrystalline aggregates with the decrease of the pH of the synthesis mixture from 13.00 to 12.30. Additional efforts were made on syntheses with pH below 12.00; however, pure ETS-4 phases were not obtained.

dx.doi.org/10.1021/cm103444e |*Chem. Mater.* 2011, 23, 1166–1173

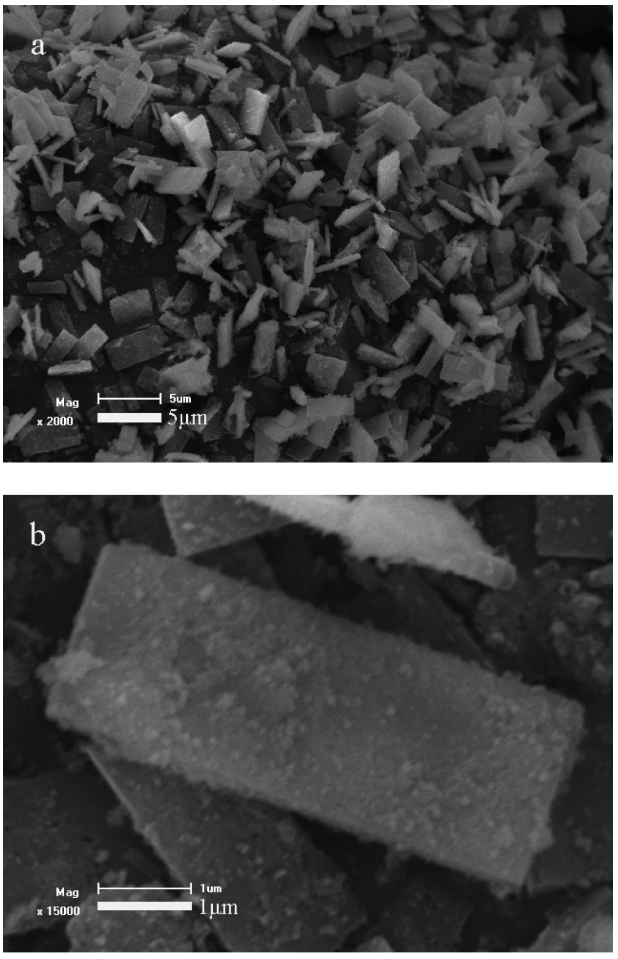

Figure 3. SEM images of ETS-4-1: (a) the monolithic crystal population and (b) the individual monolith.

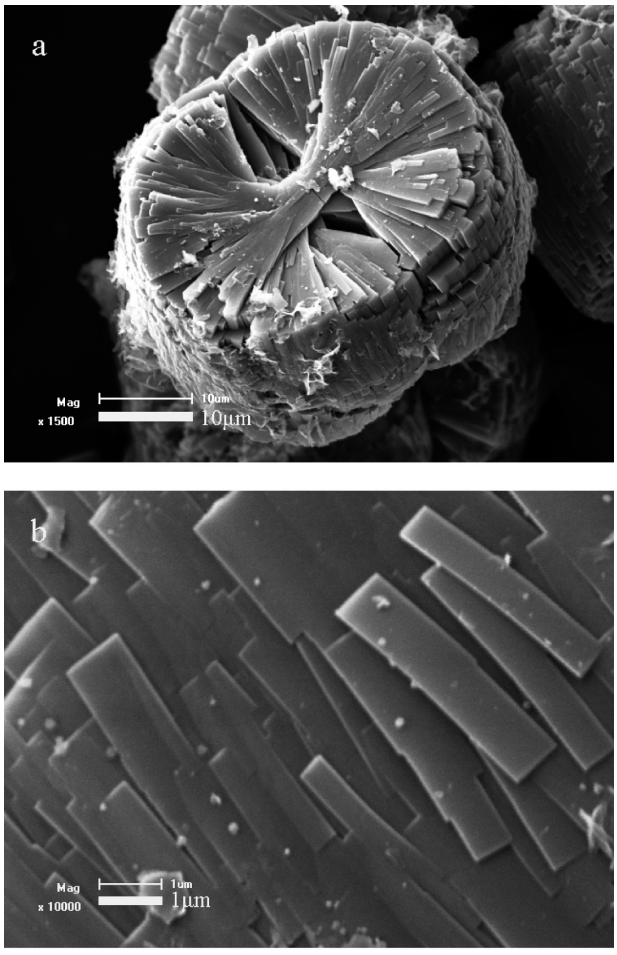

Figure 4. SEM images of ETS-4-2: (a) the polycrystalline and (b) the crystallites forming the particle.

At pH = 13.00, the synthesis mixture yielded the phase pure ETS-4-1 (Figure 3a). The majority of the crystal population was monolithic with thin rectangular plate morphology and an average dimension of 0.5 × 1.2 × 5 μm. These ETS-4-1 crystals had smooth surfaces with no intergrowths and few surface defects (Figure 3b).

When the pH of the synthesis mixture decreased to 12.70, the ETS-4-2 products changed to the form of highly intergrown polycrystalline spherulitic particles. As shown in Figure 4a, each particle was composed of two hemispheres. This morphology is consistent with earlier observations on ETS-4 synthesis.[22,43,44] The average length of the polycrystalline particles was estimated to be 40 μm, and the average thickness was 30 μm based on the SEM analysis. All the particles were uniform and homogeneous, with no significant morphology or size variation throughout the samples. In a detailed view (Figure 4b), the aggregated plate-like crystallites were rectangular prisms with an average dimension of 0.3 × 1 × 4 μm.

The lowest alkalinity of the synthesis mixture at pH = 12.30 resulted in a novel morphology. For this sample, ETS-4-3, the particles formed double-fan-like polycrystalline aggregates (Figure 5a). Each structure was composed of a myriad of tightly packed layers attached to a central hub. Compared to ETS-4-2, the length of the macro-structures of ETS-4-3 increased to 56 μm and the height decreased to 8 μm. The uniformity of the ETS-4-3 product remained good, and no large variations of spherulite size were observed. In a detailed view (Figure 5b, 5c), the aggregated crystallites appeared to be much thinner layers with triangular protrusions. The thickness of crystallites was less than 40 nm.

We attempted to measure the surface areas of the products by conventional gas adsorption methods. The degassing necessary prior to such studies led to degradation, amorphization, and partial collapse of the material, and reliable data could not be obtained. Because of the complex morphology and aggregation, estimates of surface area from particle size that might be obtained from the broadening of X-ray diffraction peaks or from electron microscopy are also not meaningful. Thus although ETS-4-3 almost certainly has a higher surface area than the other samples, these differences could not be quantified.

3.4. Photocatalytic Activity. To gain insight into the photocatalytic effect of the ETS-4 materials, the photoreaction based on the decomposition of Rhodamine B under visible light irradiation was carried out. The same experiment using a commercial TiO_2 photocatalyst Degussa P25 was also performed for comparison. A blank experiment was run in the absence of any photocatalyst to check the background. As shown in Figure 6, only a very small degree of photodegradation took place in the blank experiment, indicating the contribution of direct photolysis is negligible. After 4 h irradiation under visible light, more than 70% of the Rhodamine B was photodegraded by ETS-4-3, while the degradation for photocatalysts ETS-4-1, ETS-4-2, and P25 was much less (only 31%, 40%, and 35%, respectively). These data

dx.doi.org/10.1021/cm103444e |*Chem. Mater.* 2011, 23, 1166–1173

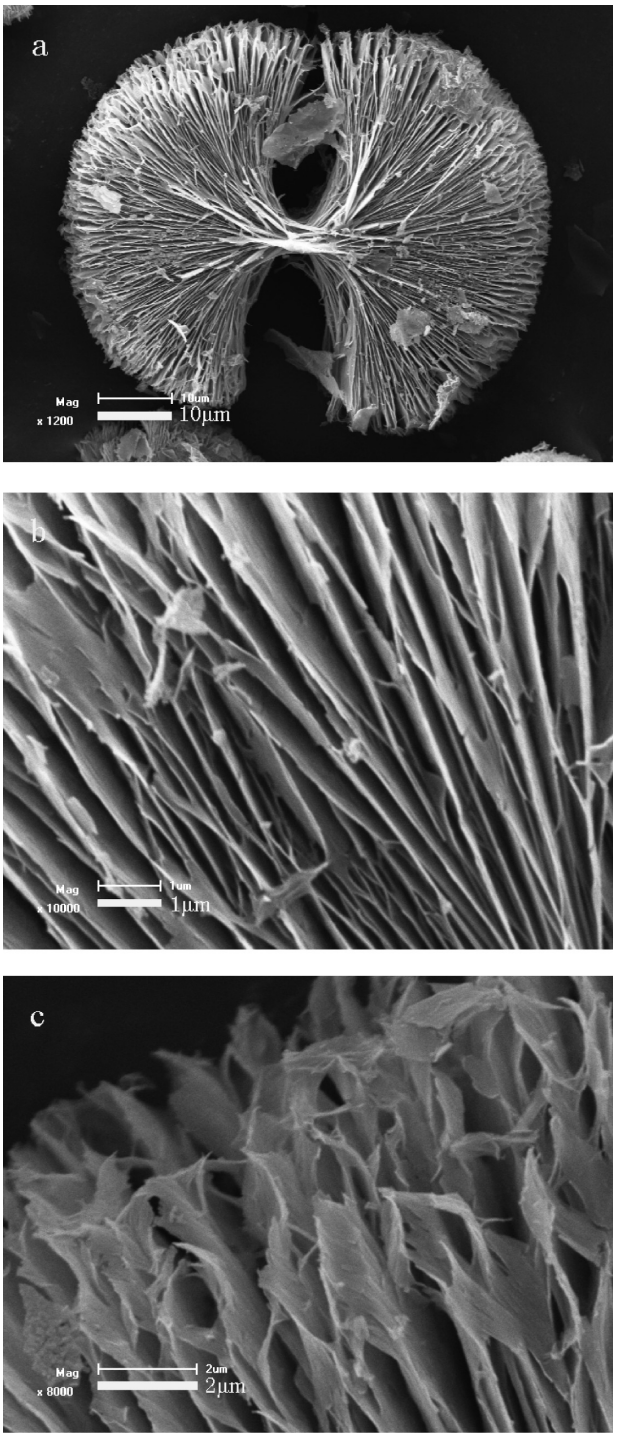

Figure 5. SEM images of ETS-4-3: (a) the polycrystalline and (b, c) the crystallites forming the particle.

show that the sample ETS-4-3 exhibits the best photodegradation activity under visible light.

The photocatalytic degradation reaction can be considered as a first-order reaction. The integrated reaction rate is $\ln(C/C_0) = -kt$, where C/C_0 is the normalized organic compound's concentration and k is the reaction rate constant. By plotting $\ln(C/C_0)$ as a linear function of irradiation time, the rate constant k that is the slope of the line can be determined for each photocatalytic reaction (see Table 2). From ETS-4-1 to ETS-4-3, the reaction rate constant increases from

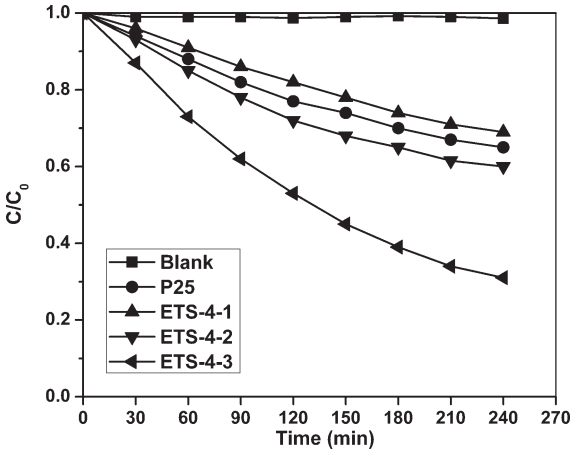

Figure 6. Photocatalytic degradation of Rhodamine B under visible light irradiation. C_0 is the initial concentration of Rhodamine B and C, the concentration at a given time.

Table 2. Photodegradation Reaction Rate Constants of Rhodamine B[a]

samples	reaction rate constant k (min^{-1})
P25	$1.83(7) \times 10^{-3}$
ETS-4-1	$1.61(4) \times 10^{-3}$
ETS-4-2	$2.20(12) \times 10^{-3}$
ETS-4-3	$5.09(11) \times 10^{-3}$

[a] Uncertainty in the last reported digit is given in parentheses.

1.61×10^{-3} to 5.09×10^{-3} min^{-1}. ETS-4-3 shows a photocatalytic activity that is about three times that of P25, while the photocatalytic activity of ETS-4-1 and ETS-4-2 is only comparable to that of P25. This phenomenon can be provisionally explained in terms of the micro/nano double-fan-like morphology of ETS-4-3 which makes Rhodamine B much easier to be adsorbed onto the surface.

It is well-known that surface Ti−OH groups play an important role in enhancing the activity of TiO_2 photocatalysts. They are considered to have two effects on enhancing the photocatalytic activity.[45,46] The Ti−OH groups are effective traps for the photogenerated holes, reducing their recombination with the electrons, and the surface OH groups allow the adsorption of O_2 from water. Then, the photoformed electrons reduce O_2 to O_2^- species, which in turn can interact with water with formation of further oxygenated radicals (mainly hydroxyl radicals ·OH). Similarly, the −O−Ti−O−Ti− chains in the ETS-4 materials can act as a TiO_2-like system able to collect the light and to generate electron−hole pairs. Moreover, the cationic radicals excited from dye molecule under visible light can readily react with hydroxyl groups. The degradation of the dyes could then be mediated by a series of redox reactions.[19,47] Consequently, the surface Ti−OH groups may improve the photocatalytic activity of ETS-4 by both photooxidation and photosensitizing mechanisms. To confirm this hypothesis, Raman spectra and hydrogen peroxide titration on the three ETS-4 materials were both performed to investigate, at least qualitatively, the concentration of the Ti−OH groups on their surfaces.

The Raman spectra of the three ETS-4 products are shown in Figure 7. In general, the three spectra are very similar to those previously reported.[48,49] The characteristic bands at 918 and 1062 cm^{-1} represent Si−O stretching modes, while the band at

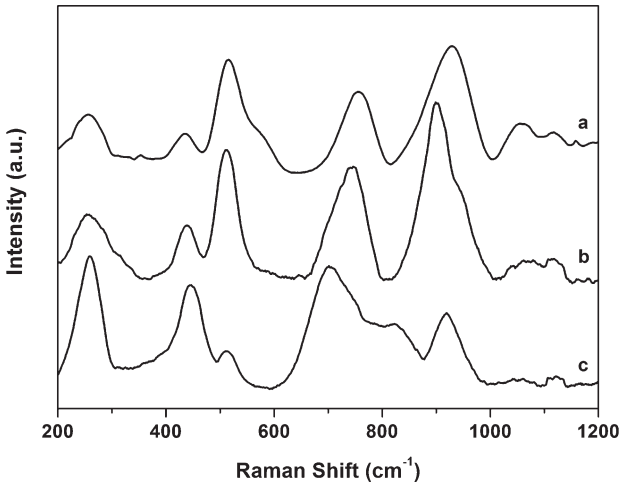

Figure 7. Raman spectra of the three photocatalysts: (a) ETS-4-1, (b) ETS-4-2, and (c) ETS-4-3.

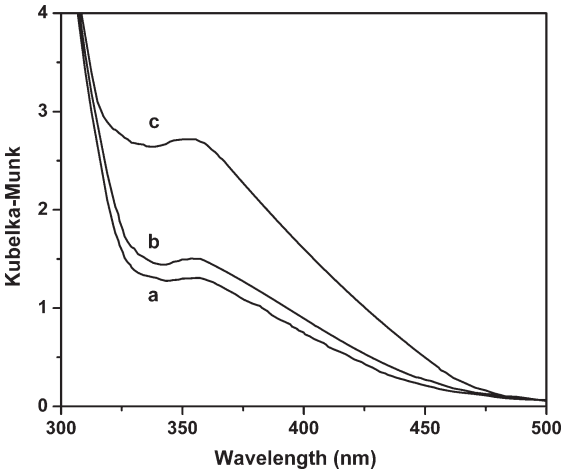

Figure 8. DRUV−vis spectra of the samples wetted with H_2O_2 solution: (a) ETS-4-1, (b) ETS-4-2, and (c) ETS-4-3.

259 cm^{-1} is predominantly due to Si−O−Ti bonding. The bands in the range 400−800 cm^{-1} are typically found in Ti−O systems. The bands at 441 and 515 cm^{-1} originate from internal modes of $[TiO_6]$ octahedra and $[TiO_5]$ pyramids. The strong peak at 741 cm^{-1} can be assigned to the −O−Ti−O−Ti− chains. However, this band broadens somewhat and shifts slightly to lower frequency, see Figure 7c. The relative magnitude of this band seems to be related to the change of morphology in the three samples. Furthermore, we also notice a new shoulder band at 824 cm^{-1}, which can be assigned to the Ti−O−H symmetrical stretching mode.[50,51] The presence of this band suggests that there is a significant number of Ti−OH groups in ETS-4-3, while the concentration of Ti−OH in ETS-4-1 and ETS-4-2 is not high enough to be detected by Raman spectroscopy. Though these observations are qualitative, they offer support to our interpretation of photocatalytic activity and thermochemistry.

As reported by Zecchina's group,[28] accessible titanol groups can be determined by DRUV−vis spectroscopy using hydrogen peroxide as a probe. The titanosilicate materials can readily react with H_2O_2 to form yellow surface species with an absorption band at 357 nm, which is attributed to the ligand-to-metal-charge-transfer transition (LMCT) from the TiOOH complexes. Figure 8 shows the DRUV−vis spectra of the three ETS-4 samples wetted with hydrogen peroxide solution. Since all the spectra were taken with H_2O_2 being in excess, the intensity of the LMCT band is proportional to the amount of the Ti−OH groups in the ETS-4 product. From ETS-4-1 to ETS-4-3, a progressive increase of the intensity of the Kubelka−Munk band at 357 nm is observed. It is therefore clear that, as a consequence of the morphology control, the number of Ti−OH groups on the surface of ETS-4-3 is increased compared to the other two ETS-4 samples. The unique double-flower-like micro/nano structure of ETS-4-3 has the most Ti−OH groups exposed on its nanoscale layer crystallite surfaces. The titration results prove the presence of the Ti−OH groups on the surface of ETS-4 and indicate the increase of the photocatalytic activity from ETS-4-1 to ETS-4-3 is probably related to the availability of titanols on the surface of the materials.

3.6. Calorimetry. The enthalpies of the drop solution of the three samples were determined by high temperature oxide melt calorimetry in molten lead borate at 973 K. As shown in Table 3, enthalpy of the drop solution decreases in the order: ETS-4-1 > ETS-4-2 > ETS-4-3. Using these values and the previously determined heats of the drop solution for Na_2O, TiO_2, SiO_2, and H_2O (also in Table 3), the molar enthalpies of formation of the three ETS-4 samples from the oxides (ΔH_f^0) were calculated through thermodynamic cycles. Taking ETS-4-3 for an example, the thermodynamic cycle used for calculation of the formation enthalpy is shown in Table 4.

A summary of the enthalpies of formation from oxides of all the three samples are shown in Table 3. All the enthalpies are exothermic, and that for ETS-4-1 (−58.15 ± 0.51 kJ/mol) is the most exothermic among the three samples, which lies about 4 kJ/mol more negative than that of ETS-4-2, and about 10 kJ/mol more negative than that of ETS-4-3. As the entropy term ($T\Delta S$) is expected to be small for condensed phase reactions, ΔG probably follows the same trend as ΔH, making the enthalpy a good indicator for the thermodynamic stability. Therefore, at ambient conditions ETS-4-1 is most stable and ETS-4-3 least. The differences in the chemical composition of the three samples may affect their enthalpies of formation. However, the enthalpies of formation per mole of H_2O and Na^+, shown in Table 4, have the same trend as that per mole of TO_2, indicating their thermodynamic stability is not obviously related to variation in the concentration of any one component.

Finally, earlier data for ETS-4[37] with potassium partly substituted for sodium, designated as ETS-4-4, are also shown in Table 3. The chemical formula for ETS-4-4 was taken as $K_{1.13}Na_{3.92}Ti_{3.07}Si_{8.17}O_{25}\cdot 8.64H_2O$. For ease of comparison, the enthalpy of formation of ETS-4-4 is also calculated on a 2-oxygen TO_2 basis with a value of −65.48 ± 1.05 kJ/mol. Thus ΔH becomes more exothermic with the partial substitution of K for Na. Similar behavior has been reported for aluminosilicate zeolites,[55] for which the enthalpy of formation becomes more negative in the sequence Ca, Li, Na, and K, reflecting increase in ionic potential (z/r) or basicity of the cations.

3.7. Relationship between Photocatalytic Activity and the Enthalpy of Formation. ETS-4-3 is the most photoactive photocatalyst of the three products, and ETS-4-3 also has the most endothermic enthalpy of formation. Given its highest intensity of the DRUV−vis band, which is directly related to the number of Ti−OH groups, there are some interesting correlations between the thermodynamics data, the photocatalytic activity, and the number of Ti−OH groups. Photocatalysis rate constants and enthalpies of formation of the three ETS-4 products

dx.doi.org/10.1021/cm103444e |*Chem. Mater.* 2011, 23, 1166–1173

Table 3. Enthalpies of the Drop Solution of the ETS-4 Materials, As Well As Constituent Oxides and Water in Molten Lead Borate at 973 K and the Enthalpies of Formation of ETS-4 Samples

samples	ΔH_{ds} (kJ/mol)	ΔH_f^0 (kJ per mol of TO_2)[a]	ΔH_f^0 (kJ per mol of H_2O)	ΔH_f^0 (kJ per mol of Na^+)
Na_2O	-113.1 ± 0.8[b]			
TiO_2	55.4 ± 0.8[c]			
SiO_2	39.1 ± 0.3[b]			
H_2O	68.9 ± 0.1[d]			
ETS-4-1	134.02 ± 0.27	-58.15 ± 0.51	-66.61 ± 0.59	-140.3 ± 1.2
ETS-4-2	127.97 ± 0.53	-54.36 ± 0.69	-65.65 ± 0.83	-135.2 ± 1.7
ETS-4-3	121.79 ± 0.40	-47.71 ± 0.57	-59.36 ± 0.71	-129.0 ± 1.5
ETS-4-4[e]		-65.48 ± 1.05	-94.73 ± 1.51	

[a] T = Ti, Si. [b] Ref 52. [c] Ref 53. [d] Ref 54. [e] Ref 37.

Table 4. Thermodynamic Cycle to Calculate the Enthalpy of Formation of ETS-4-3

reaction	enthalpy
(0.370/2) Na_2O (*sol*, 973 K) + 0.253 TiO_2 (*sol*, 973 K) + 0.654 SiO_2 (*sol*, 973 K) + 0.804 H_2O (*g*, 973 K) → $Na_{0.370}Ti_{0.253}Si_{0.654}O_2 \cdot 0.804H_2O$ (*s*, 298 K)	$\Delta H_1 = -\Delta H_{ds}$(ETS-4-3)
(0.370/2) Na_2O (*s*, 298 K) → (0.370/2) Na_2O (*sol*, 973 K)	$\Delta H_2 = (0.370/2)\ \Delta H_{ds}(Na_2O)$
0.253 TiO_2 (*s*, 298 K) → 0.253 TiO_2 (*sol*, 973 K)	$\Delta H_3 = 0.253\ \Delta H_{ds}(TiO_2)$
0.654 SiO_2 (*s*, 298 K) → 0.654 SiO_2 (*sol*, 973 K),	$\Delta H_4 = 0.654\ \Delta H_{ds}(SiO_2)$
0.804 H_2O (*l*, 298 K) → 0.804 H_2O (*g*, 973 K)	$\Delta H_5 = 0.804\ \Delta H_{ds}(H_2O)$
(0.370/2) Na_2O (*s*, 298 K) + 0.253 TiO_2 (*s*, 298 K) + 0.654 SiO_2 (*s*, 298 K) + 0.804 H_2O (*l*, 298 K) → $Na_{0.370}Ti_{0.253}Si_{0.654}O_2 \cdot 0.804H_2O$ (*s*, 298 K)	$\Delta H_6 = \Delta H_{f,\ ox}$ (ETS-4-3)
$\Delta H_{f,\ ox}$ (ETS-4-3) = $\Delta H_1 + \Delta H_2 + \Delta H_3 + \Delta H_4 + \Delta H_5 = -\Delta H_{ds}$(ETS-4-3) + (0.370/2) $\Delta H_{ds}(Na_2O)$ + 0.253 $\Delta H_{ds}(TiO_2)$ + 0.654 $\Delta H_{ds}(SiO_2)$ + 0.804 $\Delta H_{ds}(H_2O)$	

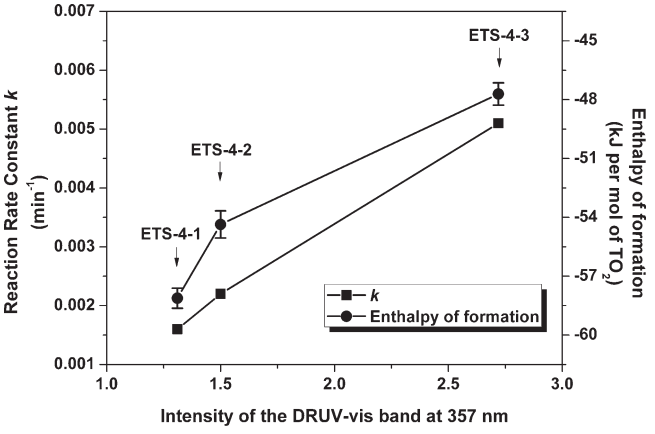

Figure 9. Photocatalytic degradation rate constants and enthalpies of formation of the three ETS-4 products versus DRUV−vis intensity.

versus DRUV−vis intensity are plotted in Figure 9. ETS-4-3 is more photoactive and has a larger number of Ti−OH groups, while the enthalpy of formation becomes less exothermic. These Ti−OH groups may increase the energy of the framework of ETS-4, so the enthalpy of formation would become more endothermic for ETS-4-3. Thus, the more endothermic the enthalpy of formation, the higher are the Ti−OH concentration and the photocatalytic activity of ETS-4.

ETS-4-3 almost certainly has a higher surface area than the other ETS-4 samples, though this could not be quantified, as discussed above. Increased surface area may contribute to the higher titanol content and photocatalytic activity, and through a surface energy term, to the enthalpy. However, the latter effect is likely to be small. Previous calorimetric study has shown, for silica MFI zeolite, that the enthalpy of formation is independent of particle size for samples with average particle diameters larger than 40 nm.[56] This observation is consistent with a small surface energy, about 0.09 J/m^2, similar to values for amorphous silica, for a series of silica zeolites of different structures, based on a combination of calorimetry and molecular modeling.[57] If the titanosilicate materials have similar surface energies, then the contribution of the surface term to the destabilization of ETS-4-3 is negligible. This strengthens the argument that the Ti−OH concentration is the major source of energetic destabilization.

4. CONCLUSION

Microporous titanosilicate ETS-4 materials with three different morphologies were hydrothermally synthesized by controlling the pH of the synthesis gel mixtures. For the first time, we synthesized the ETS-4-3 at a relatively low alkalinity (initial pH = 12.30) in a new micro/nano form of double-fan-like particles aggregated from very fine crystallites. With incremental increase of pH, other two morphologies of ETS-4 were also successfully synthesized. Changing the pH of the synthesis gel mixture can control the morphology of the ETS-4 product and the synthesis time. The photocatalytic ability of the three ETS-4 samples was studied by degradation of Rhodamine B under visible light irradiation. The ETS-4-3 photocatalyst exhibited excellent photodegradation activity, while the other two ETS-4 samples showed activity comparable to TiO_2 P25. This is caused by the increase of the number of titanol groups in ETS-4-3, compared to that of ETS-4-1 and ETS-4-2. High temperature oxide melt calorimetry determined the energetics of the ETS-4 photocatalysts. The enthalpies of formation of the three ETS-4 samples with different morphology suggest that ETS-4-3 is less thermodynamically stable than ETS-4-1 and ETS-4-2. This may be

related to its higher surface area, but the main contribution is probably from the higher concentration of Ti−OH groups. Thus, the best photocatalyst is the least stable thermodynamically. The calorimetric, spectroscopic, and photocatalytic studies all point to the titanol groups as the major source of differences in photocatalytic activity among the samples.

AUTHOR INFORMATION

Corresponding Author

*E-mail: sxliu@nankai.edu.cn (S.L.), anavrotsky@ucdavis.edu (A.N.). Phone: +86-22-23509005 (S.L.), (530) 752-3292 (A.N.). Fax: (530) 752-9307 (A.N.).

ACKNOWLEDGMENT

This work has been financially supported by the National Natural Science Foundation of China (No. 20773069), and the U.S. National Science Foundation (Grant DMR 0601892). Y.-Q. Z. would like to thank the China Scholarship Council for their sponsorship. We thank Sarah Roeske and Brian Joy (UC Davis) for their help with the electron microprobe analysis.

REFERENCES

(1) Palmisano, G.; Augugliaro, V.; Pagliaro, M.; Palmisano, L. *Chem. Commun.* **2007**, *33*, 3425–3437.

(2) Ravelli, D.; Dondi, D.; Fagnonia, M.; Albini, A. *Chem. Soc. Rev.* **2009**, *38*, 1999–2011.

(3) Hoffmann, M. R.; Martin, S. T.; Choi, W.; Bahnemann, D. W. *Chem. Rev.* **1995**, *95*, 69–96.

(4) Malato, S.; Blanco, J.; Vidal, A.; Richter, C. *Appl. Catal. B: Environ.* **2002**, *37*, 1–15.

(5) Rajeshwar, K.; Osugi, M. E.; Chanmanee, W.; Chenthamarakshan, C. R.; Zanoni, M. V. B.; Kajitvichyanukul, P.; Krishnan-Ayer, R. *J. Photochem. Photobiol. C* **2008**, *9*, 171–192.

(6) Fujishima, A.; Honda, K. *Nature* **1972**, *238*, 37–38.

(7) Linsebigler, A. L.; Lu, G. Q.; Yates, J. T. *Chem. Rev.* **1995**, *95*, 735–758.

(8) Zhang, Z. B.; Wang, C. C.; Zakaria, R.; Ying, J. Y. *J. Phys. Chem. C* **1998**, *102*, 10871–10878.

(9) Anpo, M.; Takeuchi, M. *J. Catal.* **2003**, *216*, 505–516.

(10) Thompson, T. L.; Yates, J. T. *Chem. Rev.* **2006**, *106*, 4428–4453.

(11) Chen, X.; Mao, S. S. *Chem. Rev.* **2007**, *107*, 2891–2959.

(12) Han, F.; Subba Rao, K. V.; Srinivasan, M.; Rajarathnam, D.; Naidu, R. *Appl. Catal., A* **2009**, *359*, 25–40.

(13) Rehman, S.; Ullah, R.; Butt, A. M.; Gohar, N. D. *J. Hazard. Mater.* **2009**, *170*, 560–569.

(14) Epling, G. A.; Lin, C. *Chemosphere* **2002**, *46*, 561–570.

(15) Karkmaz, M.; Puzenat, E.; Guillard, C.; Herrmann, J. M. *Appl. Catal., B* **2004**, *51*, 183–194.

(16) Wahi, R. K.; Yu, W. W.; Liu, Y. P.; Mejia, M. L.; Falkner, J. C.; Nolte, W.; Colvin, V. L. *J. Mol. Catal. A: Chem.* **2005**, *242*, 48–56.

(17) Li, D.; Haneda, H.; Hishita, S.; Ohashi, N. *Chem. Mater.* **2005**, *17*, 2588–2595.

(18) Akpan, U. G.; Hameed, B. H. *J. Hazard. Mater.* **2009**, *170*, 520–529.

(19) Liu, G.; Wu, T.; Zhao, J.; Ohidaka, H.; Serpone, N. *Environ. Sci. Technol.* **1999**, *33*, 2081–2087.

(20) Rocha, J.; Anderson, M. W. *Eur. J. Inorg. Chem.* **2000**, *5*, 801–818.

(21) Kuznicki, S. M. U.S. Patent 4,853,202, 1989.

(22) Chapman, D. M.; Roe, A. L. *Zeolites* **1990**, *10*, 730–737.

(23) Kuznicki, S. M.; Bell, V. A.; Nair, S.; Hillhouse, H. W.; Jacubinas, R. M.; Braunbarth, C. M.; Toby, B. H.; Tsapatsis, M. *Nature* **2001**, *412*, 720–724.

(24) Bordiga, S.; Palomino, G. T.; Zecchina, A.; Ranghino, G.; Giamello, E.; Lamberti, C. *J. Chem. Phys.* **2000**, *112*, 3859–3867.

(25) Mahmoodi, N. M.; Arami, M.; Limaee, N. Y.; Tabrizi, N. S. *Chem. Eng. J.* **2005**, *112*, 191–196.

(26) Krishna, R. M.; Prakash, A. M.; Kurshev, V.; Kevan, L. *Phys. Chem. Chem. Phys.* **1999**, *1*, 4119–4124.

(27) Howe, R. F.; Krisnandi, Y. K. *Chem. Commun.* **2001**, 1588–1589.

(28) Llabrés i Xamena, F. X.; Calza, P.; Lamberti, C.; Prestipino, C.; Damin, A.; Bordiga, S.; Pelizzetti, E.; Zecchina, A. *J. Am. Chem. Soc.* **2003**, *125*, 2264–2271.

(29) Usseglio, S.; Calza, P.; Damin, A.; Minero, C.; Bordiga, S.; Lamberti, C.; Pelizzetti, E.; Zecchina, A. *Chem. Mater.* **2006**, *18*, 3412–3424.

(30) Guan, G.; Kida, T.; Kusakabe, K.; Kimura, K.; Abe, E.; Yoshida, A. *Inorg. Chem. Commun.* **2004**, *7*, 618–620.

(31) Philippou, A.; Anderson, M. W. *Zeolites* **1996**, *16*, 98–107.

(32) Cruciani, G.; De Luca, P.; Nastro, A.; Pattison, P. *Microporous Mesoporous Mater.* **1998**, *21*, 143–153.

(33) Navrotsky, A. *Phys. Chem. Miner.* **1977**, *2*, 89–104.

(34) Navrotsky, A. *Phys. Chem. Miner.* **1997**, *24*, 222–241.

(35) Navrotsky, A.; Rapp, R. P.; Smelik, E.; Burnly, P.; Circone, S.; Chai, L.; Bose, K.; Westrich, H. R. *Am. Mineral.* **1994**, *79*, 1099–1109.

(36) McHale, J. M.; Auroux, A.; Perrotta, A. J.; Navrotsky, A. *Science* **1997**, *277*, 788–791.

(37) Xu, H.; Zhang, Y.; Navrotsky, A. *Microporous Mesoporous Mater.* **2001**, *47*, 285–291.

(38) Kiseleva, I.; Navrotsky, A.; Belitsky, I. A.; Fursenko, B. A. *Am. Mineral.* **1996**, *81*, 658–667.

(39) Braunbarth, C.; Hillhouse, H. W.; Nair, S.; Tsapatsis, M.; Burton, A.; Lobo, R. F.; Jacubinas, R. M.; Kuznicki, S. M. *Chem. Mater.* **2000**, *12*, 1857–1865.

(40) Nair, S.; Jeong, H.-K.; Chandrasekaran, A.; Braunbarth, C. M.; Tsapatsis, M.; Kuznicki, S. M. *Chem. Mater.* **2001**, *13*, 4247–4254.

(41) Mintova, S.; Valtchev, V.; Angelova, S.; Konstantinov, L. *Zeolites* **1997**, *18*, 269–273.

(42) Pavel, C. C.; Vuono, D.; Catanzaro, L.; De Luca, P.; Bilba, N.; Nastro, A.; Nagy, J. B. *Microporous Mesoporous Mater.* **2002**, *56*, 227–239.

(43) Yilmaz, B.; Miraglia, P. Q.; Warzywoda, J.; Sacco, A., Jr. *Microporous Mesoporous Mater.* **2004**, *71*, 167–175.

(44) Warzywoda, J.; Yilmaz, B.; Miraglia, P. Q.; Sacco, A., Jr. *Microporous Mesoporous Mater.* **2004**, *71*, 177–183.

(45) Gerischer, H.; Heller, A. *J. Phys. Chem.* **1991**, *95*, 5261–5267.

(46) Palmisano, L.; Schiavello, M.; Sclafani, A.; Martra, G.; Borello, E.; Coluccia, S. *Appl. Catal., B* **1994**, *3*, 117–132.

(47) Konstantinou, I. K.; Albanis, T. A. *Appl. Catal., B* **2004**, *49*, 1–14.

(48) Mihailova, B.; Valtchev, V.; Mintova, S.; Konstantinov, L. *Zeolites* **1996**, *16*, 22–24.

(49) Su, Y.; Balmer, M. L.; Bunker, B. C. *J. Phys. Chem. B* **2000**, *104*, 8160–8169.

(50) Byeon, S.-H.; Lee, S.-O.; Kim, H. *J. Solid State Chem.* **1997**, *130*, 110–116.

(51) Torrente-Murciano, L.; Lapkin, A. A.; Chadwick, D. *J. Mater. Chem.* **2010**, *20*, 6484–6489.

(52) Kiseleva, I.; Navrotsky, A.; Belitsky, I. A.; Fursenko, B. A. *Am. Mineral.* **1996**, *81*, 668–675.

(53) Putnam, R. L.; Navrotsky, A.; Woodfield, B. F.; Boerio-Goates, J.; Shapiro., J. L. *J. Chem. Thermodyn.* **1999**, *31*, 229–243.

(54) Robie, R. A.; Hemingway, B. S. *Thermodynamic Properties of Minerals and Related Substances at 298.15 K and abar (105 Pascals) Pressure and at Higher Temperatures*, U.S. Geological Survey Bulletin 2131; U.S. Geological Survey: Reston, VA, 1995.

(55) Navrotsky, A.; Trofymluk, O.; Levchenko, A. A. *Chem. Rev.* **2009**, *109*, 3885–3902.

(56) Moloy, E. C.; Davila, L. P.; Shackelford, J. F.; Navrotsky, A. *Microporous Mesoporous Mater.* **2002**, *54*, 1–13.

(57) Li, Q. H.; Yang, S. Y.; Navrotsky, A. *Microporous Mesoporous Mater.* **2003**, *65*, 137–143.